CAR/CXCR5-T cell immunotherapy is safe and potentially efficacious in promoting sustained remission of SIV infection

Mary S Pampusch[1*], Hadia M Abdelaal[1*], Emily K Cartwright[1], Jhomary S Molden[1], Brianna C Davey[1], Jordan D Sauve[1], Aaron K Rendahl[1], Eva G Rakasz[2], Elizabeth Connick[3], Edward A Berger[4], and Pamela J Skinner[1]

Short title: CAR/CXCR5-T cell treatment in rhesus macaques

[1] Department of Veterinary and Biomedical Sciences, University of Minnesota, St. Paul, MN 55108; [2] Wisconsin National Primate Research Center, University of Wisconsin, Madison, Madison, WI 53715; [3] Division of Infectious Diseases, University of Arizona, Tucson, AZ, 85724; [4] Laboratory of Viral Diseases, NIAID, NIH, Bethesda, MD, 20814

* Authors contributed equally to this manuscript

Corresponding author: Pamela J Skinner

                             Department of Veterinary and Biomedical Sciences

                             University of Minnesota

                             689 23rd Ave SE

                             Minneapolis, MN 55455

                             Phone: 612-624-2644

                             Email: skinn002@umn.edu

1   **Abstract**

2   During chronic human immunodeficiency virus (HIV) or simian immunodeficiency virus (SIV)

3   infection prior to AIDS progression, the vast majority of viral replication is concentrated within

4   B cell follicles of secondary lymphoid tissues. We investigated whether infusion of T cells

5   expressing an SIV-specific chimeric antigen receptor (CAR) and the follicular homing receptor,

6   CXCR5, could successfully kill viral-RNA$^+$ cells in targeted lymphoid follicles in SIV-infected

7   rhesus macaques. In this study, CD4 and CD8 T cells from rhesus macaques were genetically

8   modified to express antiviral CAR and CXCR5 moieties (generating CAR/CXCR5-T cells) and

9   autologously infused into a chronically infected animal. At 2 days post-treatment, the

10   CAR/CXCR5-T cells were located primarily in spleen and lymph nodes both inside and outside

11   of lymphoid follicles. Few CAR/CXCR5-T cells were detected in the rectum and lung, and no

12   cells were detected in the bone marrow, liver, brain, or ileum. Within follicles, CAR/CXCR5-T

13   cells were found in direct contact with SIV viral RNA+ cells. We next infused CAR/CXCR5-T

14   cells into ART-suppressed SIV-infected rhesus macaques, in which the animals were released

15   from ART at the time of infusion. These CAR/CXCR5-T cells replicated in vivo within both the

16   extrafollicular and follicular regions of lymph nodes and accumulated within lymphoid follicles.

17   CAR/CXR5-T cell concentrations in follicles peaked during the first week post-infusion but

18   declined to undetectable levels after 2 to 4 weeks. Overall, CAR/CXCR5-T cell-treated animals

19   maintained lower viral loads and follicular viral RNA levels than untreated control animals, and

20   no outstanding adverse reactions were noted. These findings indicate that CAR/CXCR5-T cell

21   treatment is safe and holds promise as a future treatment for the durable remission of HIV.

22
23

24

Author summary

A person infected with human immunodeficiency virus (HIV) has replicating virus concentrated within the follicles of lymphoid tissues. The cells needed to clear the infection, cytotoxic T lymphocytes, have limited access to follicles and, thus, the cytotoxic T lymphocytes are never completely able to clear all of the HIV from the body. In this study, we have produced immunotherapeutic T cells that home to follicles and clear infected cells. These T cells express a viral targeting chimeric antigen receptor (CAR) and a molecule called CXCR5, which leads to homing of the cells to follicles. Upon administration of these CAR T-cells to virus-infected primates, we found that the cells localized to the follicle, replicated, and directly interacted with infected cells. While the cells were not maintained in the animals for more than 4 weeks, most of the treated animals maintained lower levels of virus in the blood and follicles than untreated control animals. This study shows that this immunotherapy has potential as a treatment leading to long-term remission of HIV without the need for antiretroviral drugs.

Introduction

40   Over 38 million people worldwide live with human immunodeficiency virus (HIV)[1].

41   Antiretroviral therapy (ART) effectively reduces levels of viral replication in patients; however,

42   ART is not a cure, as it fails to fully eliminate the cellular reservoir of the virus[2–4]. Successful

43   control of HIV-1 requires life-long adherence to ART, which can be challenging for patients

44   with limited or intermittent access to healthcare. Treatment fatigue, side effects[5], and

45   inconsistent access to medications have led to unsatisfactory levels of treatment adherence that

46   range from 27–80% across various populations, in a disease requiring 95% adherence to be

47   effective. [6] Alarmingly, only 57% of people living with HIV (PLWH) in the US are virally

48   suppressed with ART[7], contributing to the public health threat, as untreated PLWH can transmit

49   virus to others. Increasingly, such transmission can lead to development of drug-resistant strains

50   of HIV[8–10]. To improve the health of individuals with HIV and to reduce community

51   transmission, there is intense global interest in fully eradicating HIV or in developing a strategy

52   for durable remission in the absence of ART[11–17].

53   Chimeric antigen receptor (CAR)-T cells have shown great promise in the treatment of certain

54   cancers, including B cell leukemia and B cell lymphomas[18–22]. CAR-T cells are of particular

55   interest in the treatment of HIV, as T cells can be engineered to specifically target the envelope

56   glycoprotein expressed on the surface of HIV-infected cells. In this study, we employed a CAR

57   that targets two independent regions of the viral glycoprotein gp120[12,23]; the CAR contains CD4

58   (domains 1 and 2) and the carbohydrate recognition domain of mannose-binding lectin (MBL).

59   The MBL prevents CD4 from acting as a viral entry receptor, the bispecific antigen recognition

60   increases the anti-viral potency of the CAR, and the use of self domains minimizes the

61   possibility of immunogenicity[23].

3

62   During chronic HIV and simian immunodeficiency virus (SIV) infections prior to AIDS

63   progression, the vast majority of viral replication concentrates within B cell follicles[24–30],

64   primarily within T follicular helper cells (Tfh)[24–26,31,32]. Free virions in immune complexes are

65   also localized in follicles through binding to follicular dendritic cells (FDC) in germinal centers

66   (GC)[33–41]. By contrast, levels of virus-specific CD8$^+$ T cells, which are critical in controlling

67   HIV and SIV infections, are found at relatively low levels within B cell follicles[26,27,42,43]. In fact,

68   we previously reported the average ratio of in vivo effector (virus-specific CD8$^+$ T cells) to target

69   (virus-infected cells) cells is over 40-fold lower in follicular (F) compartments compared to

70   extrafollicular (EF) compartments of secondary lymphoid tissues[27]. Further, we reported that

71   levels of SIV in F areas during early infection[44] and levels of SIV in both F and EF areas during

72   chronic infection are inversely correlated with levels of virus-specific CD8$^+$ T cells in these

73   compartments[27]. In addition, we found that levels of virus-specific CTL in lymphoid tissues

74   correlates with reductions in viral loads [45,46]. Migration of lymphocytes into B cell follicles is

75   directed by the binding of the chemokine receptor, CXCR5[47–49], to the chemokine ligand,

76   CXCL13[50–52], which is produced by follicular stromal cells, such as marginal reticular cells and

77   FDC, and by GC Tfh cells[53–59]. Thus, expression of CXCR5 on the surface of a CD8$^+$ T cell

78   mediates migration into B cell follicles[60,61].

79

80   We hypothesize that increasing the numbers of HIV-specific CD8$^+$ T cells in B cell follicles will

81   decrease viral replication within the follicles and lead to durable control of HIV[62,63]. In this

82   study, we tested this hypothesis in an SIV-infected rhesus macaque model of HIV infection.

83   Infusion of SIV-infected rhesus macaques (both ART-naïve and ART-suppressed) with rhesus-

84   specific (CD4-MBL)CAR/CXCR5-T cells showed preliminary evidence that the treatment was

85   safe and potentially efficacious in promoting sustained remission of SIV infection. After

86   infusion, CAR/CXCR5-T cells proliferated, accumulated in B cell follicles, interacted with viral

87   (v)RNA$^+$ cells, and showed an association with reduced levels of follicular vRNA$^+$ cells and

88   overall decrease in plasma viral load. These studies indicate that CAR/CXCR5-T cell

89   immunotherapy shows promise as a tool in the development of durable remission of HIV

90   infection without the need for life-long ART.

91

92   **Results**

93   **CAR/CXCR5-T cells home to lymphoid follicles and contact SIV-infected cells in vivo**

94   To evaluate the localization and relative abundance of CAR/CXCR5-T cells in lymphoid and

95   non-lymphoid tissues, and the relative localization within lymphoid tissues of CAR/CXCR5-T

96   cells and SIV vRNA$^+$ cells, we autologously infused CAR/CXCR5-transduced T cells into an

97   SIVmac239-chronically infected rhesus macaque and sacrificed the animal 2 days post-treatment

98   (DPT). CAR/CXCR5-T cells were labeled with the fluorescent dye Cell Trace Violet (CTV), and

99   infused into the animal at a dose of 0.35×10^8 cells/kg. Spleen, lymph node (LN), rectum, ileum,

100   bone marrow, lung, liver, and brain were collected at 2 DPT, and examined for localization of the

101   CTV-labeled cells (Figure 1a). CAR/CXCR5-T cells accumulated primarily in the B cell follicles

102   in the F and EF areas of the spleen and LN, with a few cells detected in the rectum and lung. No

103   CAR/CXCR5-T cells were detected in ileum, bone marrow, liver, or brain tissue (Figure 1a). To

104   evaluate the localization of CAR/CXCR5-T cells relative to SIV vRNA$^+$ cells, we used duplex

105   RNAScope in situ hybridization (ISH)[64–66], which allows simultaneous detection of both

106   gammaretroviral vector-transduced CAR/CXCR5-T cells and SIV-infected cells. Spleen tissue

107   sections were hybridized to two sets of probes, one that specifically binds the gammaretroviral

108   CAR/CXCR5 construct and another that specifically binds SIV vRNA (Figure 1b). In addition to

5

109   detecting SIV vRNA^{+} cells, SIV virions trapped by the follicular dendritic cells (FDC) network

110   were detected as a white haze within the B cell follicle as described previously[60,65]. The duplex

111   RNAScope ISH was combined with immunofluorescence staining to allow the delineation of F

112   and EF areas in lymphoid tissues. CAR/CXCR5-T cells were detected primarily in F areas of the

113   spleen (20.1 cells/mm^2 in F compared to 3.8 in EF) and, in some instances, were detected in

114   direct contact with SIV vRNA^{+} cells (Figure 1b). We found 4% (23/621) of SIV vRNA^{+} cells

115   were in direct contact with CAR/CXCR5-T cells.

116

117   **Infusion of CAR/CXCR5-T cells into SIV-infected rhesus macaques is safe**

118   We next investigated the safety and in vivo efficacy of CAR/CXCR5-T cell immunotherapy in

119   SIV-infected ART-suppressed animals, compared to untreated control animals. The untreated

120   and treated animal groups included male and female animals, of similar age, weight, peak viral

121   loads and CD4/CD8 frequencies (Table 1).

122

123   **Table 1: Animal information**

Group	Animal	Age (yrs)	Sex	Weight (kg)	Peak VL Post-infection	Pre-ART CD4/CD8 frequency	ART treatment (days)	Necropsy (DPT)
T0	R14025	3.6	M	5.5	3.80 x10^7	-	-	2
T1	R01093	17	F	7.6	0.94 x10^7	0.44	337	56
T1	Rh2526	9.8	F	5.0	4.74 x10^7	0.76	379	70
T1	Rh2537	13	F	8.0	0.94 x10^7	1.28	358	83
C	R12049	6.3	F	6.4	6.37 x10^7	1.06	337	56
C	R11100	7.1	F	7.4	4.62 x10^7	0.31	379	70
C	R10002	9	M	11.2	2.75 x10^7	0.77	358	83
T2	Rh2850	4.7	M	6.3	0.93 x10^7	1.08	104	308
T2	Rh2853	7.1	M	9.2	2.00 x10^7	1.29	76	77
T2	Rh2858	6.4	M	10.6	2.38 x10^7	0.68	90	328

124   CAR/CXCR5-T cells were produced using gammaretrovirus transduction of peripheral

125   mononuclear cells (PBMCs). For the first treatment group (T1), CAR/CXCR5-T cells were

126   generated using PBMCs collected from rhesus macaques during the chronic stage of infection.

127   For the second treatment group (T2), CAR/CXCR5-T cells were generated from PBMCs

128   collected prior to SIVmac251 infection. T1, T2, and control animals were suppressed with

129   antiretroviral therapy (ART) that was initiated 63–68 days post-infection. Animals were released

130   from ART at the time of CAR/CXCR5-T cell infusion and monitored for at least 60 days, as

131   outlined in the study design shown in Figure 2. Blood and tissue samples were collected over

132   time to monitor infused cells and SIV vRNA.

133   To evaluate the safety of the treatment, animals were monitored by veterinary staff twice daily

134   for any signs of pain, illness, and stress by observing appetite, stool, behavior, and physical

135   condition in response to the infused CAR/CXCR5-T cells. The animals exhibited no observable

136   adverse ill effects after receiving the immunotherapeutic cells, and their weights were unaffected

137   by the immunotherapeutic infusion. Necropsy reports noted no abnormalities in treated animals

138   beyond those typical in SIV-infected animals.

139   A Luminex assay for monitoring cytokine levels after the cell infusion showed a transient spike

140   in IL-6 and interferon gamma (IFN-γ) at 2 DPT in three of the six treated animals; and levels

141   returned to normal by 6 DPT (Fig S1a–d). Flow cytometry (Fig S1e) and quantitative polymerase

142   chain reaction (qPCR) (Fig S1f) detected cells in bronchoalveolar lavage (BAL) samples shortly

143   after infusion; however, we detected no CAR/CXCR5-T cell accumulation in lung tissues

144   (Figure 1). The cells likely accumulated in the BAL shortly after infusion due to pulmonary

145   circulation. Upon necropsy, the lungs appeared healthy. The overall health of the animals and the

146   transient nature of the cytokine spikes suggests that the infusion of autologous CAR/CXCR5-T

147   cells is safe.

148

149   **Infused CAR/CXCR5-T cells were predominantly activated central memory T cells**

150   T1 and T2 animals were infused with CAR/CXCR5-T cells at a dose ranging from $0.8–2.0 \times 10^8$

151   cells/kg (Table 2). The infused cells were a mix of CD8 and CD4 T cells. Most of the infused

152   cells expressed both the CAR and CXCR5 (range, 55–79.4%) and displayed primarily a central

153   memory phenotype (range, 50.3–73.6%) (Table 2, Fig S2). The majority of the central memory

154   cells expressed C-C chemokine receptor 7 (CCR7) (range, 44.6–93.5%), a LN homing

155   molecule[67–69].

156

157   **Table 2: Cell infusions**

Group	Animal	Cells/kg infused	%CAR/CXCR5	% CM	% CCR7+	% CD4$^+$	% CD8$^+$	% CD4$^+$CD8$^+$
T0	R14025	0.35×10^8	66.2	58.1	93.5	43.8	16.3	38.0
T1	R01093	0.8×10^8	55.0	50.3	66.5	22.3	46.5	28.8
T1	Rh2526	1.12×10^8	59.5	65.3	62.5	26.8	36.0	35.4
T1	Rh2537	0.75×10^8	57.4	66.9	59.0	42.3	27.3	28.9
T2	Rh2850	2.0×10^8	79.4	73.6	62.5	20.6	14.3	63.8
T2	Rh2853	1.06×10^8	68.6	54.5	44.6	32.3	15.3	48.3
T2	Rh2858	1.26×10^8	58.4	61.4	76.4	33.4	23.2	41.9

158

159   **CAR/CXCR5-T cell infusion associated with reductions in viral loads**

160   Viral loads were monitored after infusion of CAR/CXCR5-T cells into rhesus macaques.

161   Untreated control animals (Figure 3a) showed a rapid rise in viral loads 10 to 14 days after ART

162   cessation, followed by a slow decline over time that remained at detectable levels throughout the

8

163   56 to 83 day experiment. T1 animals (Figure 3b), in which cells were collected during chronic

164   untreated infection, showed an initial immediate spike in viral loads due to the presence of virus

165   in the infused SIV-infected transduced cells[70]. Viral loads dropped in all three treated animals—

166   reaching undetectable levels in one of the three animals—and then began to rise. For the duration

167   of the experiment, one of the three T1 treated animals maintained substantially lower viral loads

168   compared to control untreated animals, and two of the three treated animals had undetectable

169   viral loads at necropsy (56-83 DPT).

170

171   In T2 animals (Figure 3c), two of the three treated animals showed lower peak viral loads post-

172   ART release compared to control untreated animals. One-month post-infusion (27–30 DPT), the

173   viral loads in two of the three T1 and all three T2 animals were lower than untreated control

174   animals, with the median viral load of T2 being nearly 2 logs below that of the untreated control

175   animals (Figure 3d). As an exception to the study design, which was planned to maintain animals

176   for only 2–3 months post-cell infusion and ART release, we maintained two T2 animals for 10

177   months post-infusion to monitor long-term viral loads. During this time, the animals maintained

178   control of infection, with viral loads oscillating between undetectable and very low levels (Figure

179   3c). We detected similar levels of naturally occurring SIV-specific (Mamu-A1*001/Gag-CM9)

180   CD8$^+$ T cells in PBMCs of treated and untreated control animals at one-month post-infusion (Fig

181   S3). This finding suggests that the differences in viral loads between groups was not likely

182   driven by differences in the endogenous response. Overall, these data suggest that CAR/CXCR5-

183   T cell therapy is effective at reducing viral loads in SIV-infected rhesus macaques after ART

184   cessation.

185

186   **CAR/CXCR5-T cells proliferate in vivo**

187   At 2 DPT, CTV-labeled CAR/CXCR5-transduced cells showed evidence of proliferation in both

188   the EF and F areas of LNs, showing doublets of cells and cells with decreased fluorescence

189   intensity, indicating a loss of CTV with cell division. Cells within the F areas had an overall

190   lower CTV fluorescence intensity than those in the EF (Figure 4a), suggesting that they had

191   undergone further cell division. Similarly, at 2 DPT, RNAScope detection of CAR/CXCR5-T

192   cells combined with immunofluorescence staining of LNs showed clusters of CAR/CXCR5-T

193   cells at the edge of the follicles, suggestive of cell expansion (Figure 4b). These clusters were

194   detected in over 50% of the follicles (range, 49–58%). In vivo proliferation of CAR/CXCR5-T

195   cells was further confirmed at 6 DPT in LN sections in treated animals by a combination of

196   RNAScope and Ki67 antibody staining to mark T cell activation and proliferation. We detected

197   Ki67$^+$ CAR/CXCR5-T cells in both F and EF areas (Figure 4c). Levels of Ki67$^+$ CAR/CXCR5-T

198   cells showed a median of 30% (range, 9–64%) of total CAR/CXCR5-T cells in F areas and a

199   median of 36% (range, 13-44%) of total CAR/CXCR5-T cells in EF areas. Interestingly, the T2

200   animal demonstrating the greatest control (Rh2850), showed the highest percentage of F Ki67$^+$

201   CAR/CXCR5-T cells (64%) and the animal that lost control (Rh2853) showed the lowest

202   percentage of follicular Ki67$^+$ CAR/CXCR5-T cells (9%) (Figure 4d).

203

204   **CAR/CXCR5-T cells localize to the follicle and persist for up to 28 days**

205   We analyzed CAR/CXCR5-T cells in LN sections from T2 animals biopsied at 2, 6, 14, 28, and

206   60 DPT using RNAscope. There was a noticeable shift at 6 DPT to CAR/CXCR5-T cells

207   primarily accumulating within B cell follicles (Figure 5b compared to Figure 4b). Quantification

208   of CAR/CXCR5-T cells in the F and EF regions of LNs revealed that CAR/CXCR5-T cells were

209   most abundant during the first week post-infusion, followed by a decline over time (Figure 5c).

10

210   At 2 DPT, CAR/CXCR5-T cells were detected at similar levels in both F and EF areas, with a

211   median of 28 cells/mm^2 (range, 26–30 cells/mm^2) in F areas and 30 cells/mm^2 (range, 23–37

212   cells/mm^2) in EF areas (Figure 5c). At 6 DPT the cells were detected predominantly in F areas

213   with a median of 78 cells/mm^2 (range, 34–239 cells/mm^2) compared to a median of 11 cells/mm^2

214   (range, 3–38 cells/mm^2) in EF areas. (Figure 5c). At 14 DPT, the F:EF ratio increased, however,

215   the overall frequency of cells sharply declined in all treated animals, with a median of 2.3

216   cells/mm^2 (range, 0.32–7.6 cells/mm^2) in F and 0.4 cells/mm^2 (range, 0–0.57 cells/mm^2) in EF

217   areas (Figure 5c). By 28 DPT, cells were only detected in F areas of one animal (Rh2850; 1.17

218   cells/mm^2), with no cells detected at 60 DPT in any of the examined sections of the treated

219   animals (Figure 5c). Notably, the animal that lost viral control (Rh2853) showed the fastest and

220   steepest decline in levels of CAR/CXCR5-T cells over time relative to two animals that

221   controlled infection.

222

223   Most follicles in the LNs had detectable CAR/CXCR5-T cells during the first week post-

224   treatment. In fact, at 6 DPT; a median of 96% (range, 90–100%) of follicles examined had

225   CAR/CXCR5-T cells (Figure 5d). These levels declined in all animals at subsequent timepoints.

226

227   Examination of PBMCs using both flow cytometry and qPCR revealed a similar pattern of

228   CAR/CXCR5-T cell persistence. Flow cytometry analysis detected CAR/CXCR5-T in isolated

229   PBMCs up to 14–21 DPT (Figure 5e), and genomic DNA PCR detection of CAR/CXCR5-T

230   cells in PBMCs showed a similar decline in cell number by day 14 (Figure 5f). In addition, we

231   found a strong positive correlation between levels of follicular CAR/CXCR5-T cells in LN tissue

232   in situ and the frequency of CD4-MBL$^+$ CAR cells detected in PBMCs by flow cytometry (Fig

11

233   S4). This finding suggests that the cells have similar persistence in peripheral blood and tissue,

234   and that detection of CAR/CXCR5-T cells in peripheral blood may be a useful surrogate marker

235   for levels and persistence of CAR/CXCR5-T cells in lymphoid tissues.

236   **In vivo levels of viral RNA appear to be impacted by CAR/CXCR5-T cells**

237   We determined the levels of vRNA in the three T2 animals and three control animals at 28 DPT

238   (Figure 6). The two treated animals that exhibited sustained control of SIV infection (Rh2850,

239   Rh2858) showed few to no SIV vRNA^{+} cells at 28 DPT in F and EF areas compared to abundant

240   SIV vRNA^{+} cells in untreated control animals and the T2 animal that did not control the

241   infection (Rh2853) (Figure 6a and b). Notably, we detected no CAR/CXCR5-T cells that were

242   SIV vRNA[+] in the examined sections. In addition, Rh2850 and Rh2858 animals had lower

243   percentages of follicles with free virions trapped by the FDC network than untreated control

244   animals, or the treated animal that lost control (Rh2853) (Figure 6c). In fact, Rh2850 had no

245   detectible FDC associated virions in any follicles, and only one of 30 follicles showed FDC-

246   associated virions in Rh2858, whereas most follicles showed FDC trapped virions in untreated

247   control animals and the treated animal that lost control. These findings suggest that the

248   immunotherapeutic cells may have led to sustained reductions in vRNA in the treated animals.

249

250   **Discussion**

251   HIV and SIV viral replication is concentrated in lymphoid B cell follicles[24–30] during chronic

252   infection, with infected Tfh in follicles representing a major barrier to HIV eradication[24–

253   27,31,32,63]. The failure of virus-specific CD8^{+} T cells to accumulate in large numbers within the B

254   cell follicles of HIV-infected individuals and SIV-infected rhesus macaques appears to be a

12

255   major mechanism allowing for persistent follicular viral replication[26,27,32,42,43,71]. In addition,

256   increasing levels of SIV- and HIV-specific T cells within B cell follicles are associated with viral

257   control[27,72–74]. These findings led us to hypothesize that infusion of T cells engineered to co-

258   express a potent SIV-specific CAR along with the B cell homing molecule, CXCR5, will control

259   SIV-infection by reducing viral replication in follicles. We tested this hypothesis in an SIV-

260   infected rhesus macaque model of HIV, in which SIVmac251-infected animals were ART

261   suppressed prior to treatment, and ART removed on the day of treatment with CAR/CXCR5-T

262   cells. Combining a potent SIV-specific CAR with the B cell follicle homing properties of

263   CXCR5 on T cells can overcome the limitation of the endogenous virus-specific $CD8^+$T-cell

264   immune response to SIV and lead to control of viremia after ART interruption.

265

266   This study provided preliminary evidence of both the efficacy and the safety of autologous

267   CAR/CXCR5-T cell immunotherapy. CAR/CXCR5-T cells successfully homed to B cell

268   follicles and interacted with SIV-infected cells in vivo. The cells proliferated in situ and

269   accumulated primarily in F areas. Five of six treated animals showed lower viral loads at one-

270   month post-infusion and had fewer follicular $vRNA^+$ cells in LNs compared to untreated

271   animals. Apart from a transient increase in inflammatory cytokines, none of the animals infused

272   with CAR/CXCR5-immunotherapeutic T cells had an adverse reaction to the infusion. Taken

273   together, these pilot studies in the rhesus macaque model of HIV suggest that autologous

274   CAR/CXCR5-T cell therapy may be a viable tool for the treatment of HIV infection in ART-

275   suppressed individuals after ART cessation.

276

277   This study used cells collected either during chronic infection (T1) or collected prior to infection

278   (T2) to produce CAR/CXCR5-T cells. We did not use cells from ART-suppressed animals

279   because we and others observed reductions in the transduction efficiency of T cells from ART-

280   treated subjects[70,75]. Such decreased transduction efficiency may be due to interference with

281   reverse transcription and integration of the gammaretroviral vector by the residual ART drugs.

282   Expression of the transgenes in T cells from ART-suppressed subjects may be improved with

283   alterations in the transduction protocol, use of vectors for virus production that are not impacted

284   by ART drugs or through the use of alternative methods of gene transfer[70].

285

286   Our previous studies examining the function of (CD4-MBL)CAR/CXCR5-T cells indicated that

287   the CXCR5 molecule facilitated migration to B cell follicles both in vitro and ex vivo[61]. Ayala et

288   al. previously showed that CXCR5 expression on T cells induces cell migration into lymphoid

289   follicles in vivo in rhesus macaques[60]. This study extends those findings, demonstrating that the

290   addition of an anti-viral CAR on CXCR5-transduced T cells leads to similar migration and

291   accumulation within B cell follicles.

292

293   Shortly after infusion, CAR/CXCR5-T cells proliferated in vivo. At 2 DPT, we detected clusters

294   of replicating CAR/CXCR5-T cells often located at the edge of the follicles. The CAR/CXCR5-

295   T cells appeared to replicate initially next to follicles, then enter into the follicles as suggested by

296   progressively decreasing CTV staining from EF to F areas. Ki67 staining confirmed the in vivo

297   proliferation of CAR/CXCR5-T cells and showed that the cells were replicating in both EF and F

298   areas. It is unclear what cues instigated the in vivo proliferation. Factors that may have

299   contributed include: the culturing conditions prior to infusion, the detection of antigen in vivo by

14

300   CAR/CXCR5-T cells, or other proliferation cues. To our knowledge, this study is the first to

301   visually confirm the in vivo expansion of autologous SIV-specific CAR T cells in ART-

302   suppressed and -released animals without adding exogenous antigen.

303

304   We have previously shown that CAR/CXCR5-T cells readily target and suppress SIV-infected T

305   cells in vitro[61]. This in vivo study showed detection of (CD4-MBL)CAR/CXCR5-T cells directly

306   interacting with SIV-infected cells within lymphoid follicles. These interactions provide

307   evidence that CAR/CXCR5-T cells specifically targeted SIV vRNA$^+$ cells, and likely led to the

308   death of these infected cells. Since the CAR does not require antigen presented in the context of

309   an MHC molecule, it is possible that CAR/CXCR5 T cells may not only attack HIV/SIV

310   producing T cells in vivo but may also act to clear the FDCs containing bound SIV. However, it

311   was recently reported that CD4-MBL CAR-T cells did not target FDCs bearing HIV bound

312   immune complexes in vitro[76], suggesting that the CAR-T cells may not target FDC bearing virus

313   in vivo. We noted little or no virus particles trapped by FDC in the LNs of the T2 animals that

314   went on to show long-term control of the virus and cannot rule out the possibility that the

315   CAR/CXCR5-T cells were able to recognize and remove FDC bearing virions. Alternatively, and

316   perhaps more plausibly, the killing of SIV-producing cells in follicles may have led to a

317   reduction in the seeding of FDCs with virions, explaining the absence of SIV loaded FDC.

318

319   Historically, engineering CD8$^+$ T cells to express CD4 presents a challenge for HIV treatment

320   due to the likelihood that enhanced CD4 expression would make the transduced CD8$^+$ T cells

321   susceptible to HIV infection[12,77–80] owing to abundant expression of the CCR5 coreceptor[81]. To

322   overcome this issue, we used a bispecific CAR construct, (CD4-MBL)CAR/CXCR5[12,23]. The

15

323 MBL moiety of the CAR creates a steric hindrance that prevents the CD4 of the CAR from

324 acting as an entry receptor[23]. Nonetheless, CD4+ T cells transduced with CAR and CXCR5 are

325 presumably susceptible to SIV/HIV infections. Interestingly, we detected no SIV vRNA in

326 CAR/CXCR5 cells in the examined sections. These data suggest that either the CD4+

327 CAR/CXCR5-T cells were not readily infected or, if infected, were rapidly cleared.

328

329 Infusion of CAR/CXCR5-T cells appeared to cause no ill effects in the animals, as indicated by

330 veterinary health records and by unremarkable necropsy reports including a lack of inflammation

331 in the lung. Three of six treated animals showed an increase in serum IL-6 and IFN-γ at 2 DPT;

332 however, the effect was transient, did not manifest as detectable illness, and may have actually

333 been a measurement of early in vivo activity of the CAR-T cells[82–84]. The animals exhibited no

334 neurotoxic symptoms or signs of fever and weight loss, which were described in a recent study

335 of neurotoxicity following CAR-T cell infusion[85]. Previous rhesus macaque adoptive transfer

336 studies found that a significant fraction of the infused T cells localize to the lung with limited to

337 undetectable persistence in blood or lymphoid tissues[86,87]. In lung tissues, we detected very low

338 levels of CTV-CAR/CXCR5-T cells in vivo from the animal sacrificed at 2 DPT. We detected

339 CAR/CXCR5-T cells in BAL fluid in four of the six treated animals between 2 and 14 DPT;

340 however, this accumulation was transient as no cells were detected at 28 DPT.

341

342 We have previously shown that CAR/CXCR5-T cells produced from chronically infected

343 animals, while effective at suppressing SIV in culture, retain residual virus[70]. T1 animals

344 received CAR/CXCR5-T cells generated using PBMCs from chronically SIV-infected animals.

345 Thus, it was not surprising that T1 animals showed a spike in viral load immediately post-

16

346   infusion. Nonetheless, even with the infusion of virus along with the CAR/CXCR5-T cells, one

347   of the three treated animals maintained viral load below 10^4 copies/mL throughout the study, and

348   two had undetectable viral loads at necropsy.

349

350   While our animal numbers per group were too small to perform statistical analyses between

351   groups, we found that two of the three T2 animals maintained viral loads below 10^4 copies/mL

352   for the entire study, with levels below or near the level of detection for up to 10 months post-

353   infusion. We detected very little to no SIV RNA$^+$ cells in both F and EF areas of LNs from these

354   two animals one-month post-treatment. Since the CAR/CXCR5-T cells did not persist beyond

355   one month, it is unclear how the animals maintained control for the subsequent months.

356   However, it is rare for rhesus macaques to spontaneously control viral rebound after interruption

357   of ART [88,89]. The CAR/CXCR5-T cells may have effectively suppressed and slowed down SIV

358   recrudescence post-ART release, allowing the endogenous immune response to be effective in

359   maintaining low or undetectable viral loads in these animals. The T2 animal that did not control

360   viral infection showed several important differences from the two controller animals. In the non-

361   controlling animal, the infused cells showed decreased expansion in vivo, declined more quickly,

362   and were more abundant in the BAL. Additionally, the non-controlling animal had a relatively

363   lower percentage central memory cells and lower CCR7 expression than the animals that

364   controlled plasma viremia post-infusion. It is possible that, due to differences in central memory

365   phenotype, the cells did not persist as long, or were not present at a sufficient levels, at the time

366   of viral recrudescence, and failed to exert an effect on viral load.

367

17

368   CAR/CXCR5-T cells accumulated predominantly in lymphoid tissues, where they reached peak

369   accumulation at 6 DPT and persisted for up to 28 days. The preferential homing of infused

370   CAR/CXCR5-T cells to lymphoid tissues in our study may be due to relatively high frequency of

371   central memory cells (median 63%)[90]. Overall, no CAR/CXCR5-T cells were found in the blood

372   or tissues past 28 DPT. Many adoptive transfer studies utilize a lymphodepletion regimen using

373   cytotoxic agents, such as Cytoxan, to create room for the adoptively transferred cells to

374   implant[91–94], and such a conditioning regimen in future studies may allow greater expansion and

375   persistence of CAR/CXCR5-T cells. Alternatively, persistence might be improved by the

376   addition of antigen-expressing cells at, or shortly after, the time of CAR-T cell infusion to

377   stimulate CAR-T cells in vivo, as was recently reported by Rust et al[74].

378

379   To achieve better long-term control of infection, CAR/CXCR5-T cell immunotherapy could also

380   be combined with other strategies aimed at eliminating the HIV/SIV reservoir. Such therapies

381   might include latency reversal agents[62,95] or agents that modify the immune system[96], such as an

382   IL-15 superagonist[97].

383

384   These studies provide preliminary evidence of the safety and efficacy of CAR/CXCR5-T cells in

385   a rhesus macaque model of HIV. Future studies with larger numbers of animals are essential to

386   definitively determine the safety and efficacy of this intervention. With their ability to localize to

387   the site of viral replication and to interact with virally infected cells, these immunotherapeutic

388   cells have the potential to play an important role in the long-term cure of HIV infection without

389   the use of life-long ART.

Materials and Methods

Animal Study Design

The studies used 10 rhesus macaques that were positive for the class I allele *Mamu-A1*001* but

negative for *Mamu-B*008* and *Mamu-B*017:01*. Rhesus macaques were housed at the

Wisconsin National Primate Research Center (WNPRC). All procedures were approved by the

University of Wisconsin-Madison College of Letters and Sciences and Vice Chancellor for

Research and Graduate Education Centers Institutional Animal Care and Use Committee

(IACUC protocol number G005529). The animal facilities of the Wisconsin National Primate

Research Center are licensed by the US Department of Agriculture and accredited by AAALAC.

Animals were monitored twice daily by veterinarians for any signs of disease, injury, or

psychological abnormalities. At the conclusion of the study, animals were humanely euthanized

by anesthetizing with ketamine (at least 15 mg/kg IM) or other form of WNPRC veterinary

approved general anesthesia followed by an IV overdose (at least 50 mg/kg or to effect) of

sodium pentobarbital or equivalent as approved by a WNPRC veterinarian. Death was defined

by stoppage of the heart as determined by a qualified and experienced person using a stethoscope

to monitor heart sounds from the chest area, as well as all other vital signs, which can be

monitored by observation.

The initial treated animal was chronically infected with SIVmac239 for 20 months prior to

treatment. The animal was necropsied at day 2 post-infusion to determine the abundance and

localization of the infused cells. Pilot study 1 and 2 treated animals (T1 and T2) and control

untreated animals (C) (n=3 per group) were infected intrarectally with SIVmac251 (1×10^8 viral

RNA). ART consisting of 5.1 mg/kg Tenofovir Disoproxil Fumerate (TDF) (Gilead), 40 mg/kg

Emtricitabine (FTC) (Gilead) and 2.5 mg/kg Dolutegravir (DTG) (Viiv) was formulated at Beth

19

414   Israel Deaconess Medical Center (BIDMC). ART was initiated at day 63–68 post-infection and

415   continued daily until the day of cell infusion. Blood samples were drawn biweekly to monitor

416   viral loads, and all animals had undetectable viral loads at the time of infusion. Animals were

417   ART-suppressed for times indicated in Table 1. PBMCs were collected by density gradient

418   centrifugation from blood draws either post-infection for T1 or pre-infection for T2. PBMCs

419   were cryopreserved in CryoStor CS5 (BioLife Solutions Inc.) at a concentration between 4 and

420   20 million cells/mL and transported and stored in liquid nitrogen until use.

421

422   *Cell manufacturing and infusion*

423   The CD4-MBL CAR/ CXCR5 construct was described previously[61]. The bi-specific CAR

424   contains rhesus CD4 and MBL domains, which leads to specificity for SIV, linked to

425   extracellular hinge, transmembrane and co-stimulatory domains of rhesus CD28[12,23] . The

426   follicular homing receptor, CXCR5, is linked to the CAR with a self-cleaving peptide, P2A.

427   Gammaretroviruses were produced by lipofectamine-mediated transfection of 293T cells[61]. CD4-

428   MBL CAR/CXCR5-T cells were manufactured using the CD4-MBL CAR/CXCR5

429   gammaretrovirus as outlined previously[70,98]. Prior to infusion, cells were stained with CTV, an

430   intracellular fluorescent dye, resuspended at a density of 2×10^7 cells/mL in RPMI for T0 and in

431   PBS containing 10% autologous serum for all other animals, packed on ice and transported to the

432   WNPRC. The CAR/CXCR5-T cells were infused intravenously over 20 min while the animals

433   were sedated. A veterinarian was present during the entire infusion. The dose of cells ranged

434   from 0.35 to 2×10^8 cells/kg (Table 2). Following infusion, animals were evaluated for signs of

435   pain, illness, and stress observing appetite, stool, typical behavior, and physical condition by the

436   staff of the Animal Services Unit at least twice daily. The weight of the animals was monitored

437   routinely throughout the protocol.

20

438

Tissue, blood, and cell collection

Blood samples were drawn for viral load determination immediately before and after infusion

and on days 2, 6, 10, 14 and then biweekly until necropsy. Complete blood counts (CBC) were

monitored biweekly throughout the experiment. LN biopsies and BAL samples were collected on

days 2, 6, 14, 28 and 60–69 post-infusion. Colon and rectal biopsies were collected on days 2,

14, 28 and 60–69 post-infusion. Animals were necropsied between day 69 and 302 post-infusion.

Viral load determination

Viral loads were measured by Virology Services (WNPRC). vRNA was isolated from plasma

samples using the Maxwell Viral Total Nucleic Acid Purification kit on the Maxwell 48RSC

instrument (Promega, Madison WI). vRNA was then quantified using a highly sensitive qRT-

PCR assay based on the one developed by Cline et al.[99]. RNA was reverse transcribed and

amplified using TaqMan Fast Virus 1-Step Master Mix qRT-PCR Master Mix (Invitrogen) on

the LightCycler 480 or LC96 instrument (Roche, Indianapolis, IN) and quantified by

interpolation onto a standard curve made up of serial ten-fold dilutions of in vitro transcribed

RNA. RNA for this standard curve was transcribed from the p239gag_Lifson plasmid, kindly

provided by Dr. Jeffrey Lifson, (NCI/Leidos). The final reaction mixtures contained 150 ng

random primers (Promega, Madison, WI), 600 nM each primer and 100 nM probe. Primer and

probe sequences are as follows: forward primer: 5′- GTCTGCGTCATCTGGTGCATTC-3′,

reverse primer: 5′-CACTAGCTGTCTCTGCACTATGTGTTTTG-3′ and probe: 5′-6-

carboxyfluorescein-CTTCCTCAGTGTGTTTCACTTTCTCTTCTGCG-BHQ1-3′. The reactions

cycled with the following conditions: 50°C for 5 min, 95°C for 20 s followed by 50 cycles of

95°C for 15 s and 62°C for 1 min. The limit of detection of this assay is 100 copies/mL.

21

462

463   *Flow cytometry*

464   Multiparametric flow cytometry was performed on fresh, transduced PBMCs and on thawed

465   PBMCs or BAL cells collected post-infusion with monoclonal antibodies cross-reactive in rhesus

466   macaques to detect (CD4-MBL)CAR/CXCR5-T cells and SIV-specific T cells. Cells were

467   incubated with Live/Dead NIR (Invitrogen); Alexa Fluor 700 mouse anti-human CD3 (SP34-2),

468   FITC, Brilliant Violet 650 mouse anti-human CD4 (M-T477), Brilliant Violet 510 mouse anti-

469   human CD8 (RPA-T8), PerCP/Cy5.5 mouse anti-human CD95 (DX2) and Brilliant Violet 605

470   mouse anti-human CD28 (28.2) (BD Biosciences); Phycoerythrin (PE) mouse anti-human

471   CXCR5 (MU5UBEE) (eBiosciences); MBL (3E7) (Invitrogen) conjugated to Alexa Fluor 647.

472   To detect SIV-specific CD8$^+$ T cells, samples were incubated with PE-labeled GAG-CM9 (NIH

473   Tetramer Core) at 37°C for 15 min.

474

475   *CAR/CXCR5-T cell PCR*

476   DNA qPCR was used to determine the quantity of CAR-T cells in PBMCs and BAL. Genomic

477   DNA was isolated from freshly thawed PBMCs or BAL collected post-infusion using the

478   DNeasy Blood and Tissue kit (Qiagen). PCR primers were designed to specifically bind to the

479   junction of the CD4 and MBL fragments of the CAR to avoid recognition of endogenous CD4 or

480   MBL. The assay included 300 nM concentrations of the following primers:

481   CAR forward primer 5′-ATATTGTGGTCCTGGCCTTTCA-3′; CAR reverse primer 5′-

482   AAGAATTTGTTTCCGACCTGCC-3′; albumin forward primer 5′-

483   TGCATGAGAAAACGCCAGTAA-3′; albumin reverse primer 5′-

484   ATGGTCGCCTGTTCACCAA-3′. PCR was run on a CFX96 thermal cycler (BioRad) with a

485   program of one cycle of denaturation at 95°C for 2 min, followed by 40 cycles of 95°C for 10 s

22

486   and 60°C for 30 s. An amplified DNA fragment of the CAR was used in a standard curve to

487   determine the copy number of the CAR. Albumin, which is present as two copies per cell, was

488   used to determine cell number. The limit of detection was 2 copies of CAR DNA per 10^5 cells.

489

490   *Luminex assay*

491   Serum samples were stored at -80°C prior to analysis. Samples were tested by the Cytokine

492   Reference Laboratory (University of Minnesota) using the magnetic bead set PRCYTOMAG-

493   40K (EMD Millipore). Samples were analyzed for Non-Human Primate (NHP)-specific TNFα,

494   IFNγ, IL-6 & IL-2 using the Luminex platform and performed as a multi-plex. Fluorescent color-

495   coded beads coated with a specific capture antibody were added to each sample. After incubation

496   and washing, biotinylated detection antibody was added followed by phycoerythrin-conjugated

497   streptavidin. The beads were read on a Luminex instrument (Bioplex 200). Samples were run in

498   duplicate and values were interpolated from five-parameter fitted standard curves.

499

500   *Singleplex RNAScope in situ hybridization and immunohistochemistry*

501   RNAScope in situ hybridization utilized the 2.5 HD Reagent RED kit (Advanced Cell

502   Diagnostics) as described previously[65,66,100] with modifications. FFPE tissue sections (5 µm) on

503   slides were deparaffinized by baking 1 h at 60°C, rinsing in xylene followed by absolute ethanol

504   and air-drying. Sections were boiled in RNAScope® 1× Target Retrieval buffer (Advanced Cell

505   Diagnostics) for epitope retrieval. Sections were then washed in dH_2O, dipped in absolute

506   ethanol and air-dried. Following a protease pretreatment, sections were rinsed with dH_2O and

507   hybridized overnight at 40°C with one of the following probes (all from Advanced Cell

508   Diagnostics): SIVmac239 no-env antisense probe or a custom-made probe for the

23

509 gammaretroviral vector to detect the CAR/CXCR5-transduced cells, DapB probe as a negative

510 control probe or Macaca mulatta peptidylprolyl isomerase B (cyclophilin B) probe served as a

511 positive control. Sections were then washed with $0.5\times$ RNAScope wash buffer (Advanced Cell

512 Diagnostics) and incubated with amplification reagents (1-6) according to the manufacturer's

513 instructions. For chromogenic detection, sections were incubated with 120 µL of fast Red

514 chromagen solution and washed as recommended by the manufacturer. For immunofluorescence

515 staining, sections were blocked with 4% normal goat serum (NGS) and incubated overnight with

516 the following primary antibodies: mouse-anti-human CD20 (Clone L26, Biocare), mouse-anti-

517 CD68 (KP1; Biocare), rabbit anti-CD20 (Polyclonal, Thermo Scientific), rabbit anti-CD3 (SP7;

518 Labvision/Thermo Scientific), rabbit anti-CD4 (EPR6855; Abcam), or rabbit anti-Ki67 (Clone

519 SP6, Invitrogen/Thermo Scientific). Goat secondary antibodies (Jackson Immunoresearch

520 Laboratories) against mouse, rabbit, or human IgM conjugated to Alexa Fluor[TM] 488, Alexa

521 Fluor[TM] 647 or Cy5 were used. Sections were counterstained with 1µg/mL DAPI and mounted in

522 Prolong® Gold (ThermoFisher Scientific).

523

524 *Duplex in situ hybridization combined with immunofluorescence*

525 For simultaneous visualization of both SIV vRNA and CAR/CXCR5-transduced cells, the

526 RNAScope multiplex fluorescent kit V2 (Advanced Cell Diagnostics) was used with the opal

527 fluorophores system (Akoya Bioscience) according to the manufacturer's instructions and as

528 described previously[66] with some modifications. In brief, 5µm FFPE tissue sections on slides

529 were deparaffinized as described above. Sections were pretreated with H_2O_2 (to block

530 endogenous peroxidase activity) and washed in dH_2O. Heat-induced epitope retrieval was

531 achieved by boiling sections in RNAScope® $1\times$ target retrieval buffer (Advanced Cell

532   Diagnostics). Sections were washed, dehydrated in absolute ethanol, and air-dried. Sections were

533   incubated with protease solution, rinsed twice in dH_2O and incubated with pre-warmed premixed

534   target probes (all from Advanced Cell Diagnostics) in which SIVmac239 no env antisense probe

535   channel 2 (C2) was diluted in the custom-made probe for the gammaretroviral vector to detect

536   the CAR/CXCR5-transduced cells channel 1 (C1) at C2: C1 1:50 ratio overnight at 40°C.

537   Sections were washed with a 0.5× RNAScope wash buffer. Amplification and HRP-C1 and

538   HRP-C2 signal development were performed as recommended by the manufacturer with the

539   modification of the use of 0.5× RNAScope wash buffer instead of 1× RNAScope wash buffer

540   and use of a 1:150 dilution of Opals (all from Akoya Bioscience) instead of 1:1500. Opal™ 570

541   and Opal™ 690 were used for C1 and C2, respectively. For immunofluorescence staining,

542   sections were washed twice in TBST (TBS- tween 20–0.05% v/v), blocked in 10% NGS- TBS-

543   1% BSA and incubated with primary antibodies diluted in TBS-1% BSA for 1 h at RT. Primary

544   antibodies included the same antibodies described in Singleplex vRNA in situ hybridization

545   combined with immunofluorescence. The sections were washed and incubated with secondary

546   antibodies, Opal Polymer HRP Ms + Rb for 10 min at RT. After washing, the sections were

547   incubated with Opal™ 520 diluted 1:150 in the multiplex TSA buffer (Advanced Cell

548   Diagnostics) for 10 min at RT. After washing, sections were counterstained with 1µg/mL DAPI

549   and mounted in Prolong® Gold (ThermoFisher Scientific).

550

551   *Quantitative image analysis for RNAScope*

552   Sections were imaged using a Leica DM6000 confocal microscope. Montage images of multiple

553   512×512 pixels were created and used for analysis. F and EF areas were delineated using Leica

554   software with B cell follicle areas identified morphologically as clusters of closely aggregated

25

555   brightly stained CD20$^+$ or IgM$^+$ cells. Some sections were co-stained with goat anti-human IgM-

556   AF647 (Jackson ImmunoResearch) and mouse-anti-human CD20 antibodies (clone L26, Biocare

557   Medical, Inc.) to confirm that both antibodies co-localized similarly in B cell follicles. Cell

558   counts were done using LAS X (Leica confocal) software; each cell was demarcated using a

559   Leica software tool to avoid counting the same cell twice. Leica software was used to measure

560   the delineated areas for cell counts. To determine the percentage of follicles that had

561   CAR/CXCR5-T cells over time post-infusion, a total of 790 follicles were evaluated for presence

562   of CAR/CXCR5-T cells with a median of 302 follicles (range, 172–316) per animal. To

563   determine the levels of CAR/CXCR5-T cells/mm^2 in follicular areas, over time post-infusion, a

564   median of 8.4 mm^2 (range, 6.8–8.9 mm^2) of follicular area was analyzed with a total of 172

565   follicles analyzed with a median of 57 follicles (range, 48–67) per animal. In addition, a total of

566   190 follicles were examined to determine the percentage of follicles that had a cluster of

567   expanding CAR/CXCR5-T cells at the edge of the follicle at 2 DPT, with a median of 95

568   follicles (range 90–100). To determine the percentage of follicles with free virions bound by

569   FDC over time post-infusion, a total of 518 follicles with a median of 146 follicles (range 140–

570   232) per animal. To determine the levels of SIV RNA$^+$ cells/mm^2 in follicular areas, over time

571   post-infusion, a median of 6.46 mm^2 (range 5.48–6.84 mm^2) of follicular area was analyzed with

572   a total of 131 follicles analyzed with a median of 45 follicles (range 38–48) per animal. To

573   determine levels of CAR/CXCR5- T cells/mm^2 and level of SIV RNA$^+$ cells/mm^2 in treated

574   animals, a median of 19.9 mm^2 (range of 15.7–34 mm^2) of EF areas were analyzed per animal.

575   To confirm the specificity of the custom-made probe that we designed to detect the

576   gammaretroviral CAR/CXCR5 construct and to determine the level of SIV vRNA$^+$ cells in F

577   areas, LN tissues from three untreated control animals were hybridized to the custom made probe

26

578   and an SIV probe; a median of 2.36 mm^2 (range 0.79–2.99 mm^2) of follicular area was analyzed

579   with a total of 53 follicles analyzed with a median of 22 follicles (range 5–26) per animal. To

580   determine the level of SIV RNA$^+$ cells/mm^2 in untreated control animals, a median of 3.6 mm^2

581   (range of 0.68–9.3 mm^2) of EF areas was analyzed per animal.

582

583   *Immunohistochemistry and analyses*

584   Indirect immunohistochemistry was performed on fresh tissue specimens shipped overnight,

585   sectioned with a compresstome[101] and stained as described previously[102–104]. Briefly, sections

586   were stained with 0.4 µg/mL rabbit -anti-human CD20 polyclonal antibodies (Neomarkers) and 2

587   µg/mL rat-anti-human CD3 antibodies (clone MCA1477, BioRad). Then, sections were stained

588   with secondary antibodies by incubating with 0.3 µg/mL Alexa Fluor^{TM} 488-conjugated goat-

589   anti-rabbit antibodies, and 0.2–0.3 µg/mL Cy5-conjugated goat anti-rat antibodies overnight at

590   4°C. Secondary antibodies were obtained from Jackson ImmunoResearch Laboratories (West

591   Grove, PA). Sections were imaged using a Leica DM6000 confocal microscope. Montage

592   images of multiple 512×512 pixels were created and used for analysis. Confocal z-series were

593   collected in a step size of 3 µm. Images were opened and analyzed in LAS X (Leica confocal)

594   software directly. We used the LAS X software to create montages of multiple projected

595   confocal serial z-scans. Follicular areas were identified morphologically as clusters of brightly

596   stained, closely aggregated CD20$^+$ cells. F and EF areas were delineated and measured using

597   LAS X software. Areas were not included if they showed loosely aggregated B cells that were

598   ambiguous. To prevent bias, the yellow CTV channel was turned off when F and EF areas were

599   delineated. Cell counts were performed on single z-scans.

600

601   *Statistical analyses*

602   Statistical analyses utilized GraphPad Prism 8.3.0 for Windows (GraphPad Software, San Diego,

603   CA). Specific tests are indicated in the figure legends. Correlations were determined using

604   Spearman's correlation, assuming independence.

605

28

625

626   **Author contributions**

627   **Conceptualization**: Pamela Skinner

628   **Data curation**: Mary Pampusch, Hadia Abdelaal

629   **Formal analysis**: Mary Pampusch, Hadia Abdelaal, Emily Cartwright, Aaron Rendahl

630   **Funding acquisition**: Eva Rakasz, Elizabeth Connick, Edward Berger, Pamela Skinner

631   **Investigation**: Mary Pampusch, Hadia Abdelaal, Emily Cartwright, Jhomary Molden, Brianna

632   Davey, Jordan Sauve

633   **Methodology**: Mary Pampusch, Hadia Abdelaal

634   **Project Administration**: Mary Pampusch, Pamela Skinner

635   **Resources:** Eva Rakasz, Edward Berger, Pamela Skinner

636   **Supervision**: Eva Rakasz, Elizabeth Connick, Edward Berger, Pamela Skinner

637   **Visualization**: Mary Pampusch, Hadia Abdelaal, Emily Cartwright, Jhomary Molden, Brianna

638   Davey

639   **Writing-original draft**: Mary Pampusch, Hadia Abdelaal, Pamela Skinner

640   **Writing- review and editing:** Emily Cartwright, Eva Rakasz, Elizabeth Connick, Edward

641   Berger

642

643
644

References

1. WHO | HIV/AIDS. *WHO* (2020).

2. Zhang, L. *et al.* Quantifying Residual HIV-1 Replication in Patients Receiving Combination Antiretroviral Therapy. *N. Engl. J. Med.* **340**, 1605–1613 (1999).

3. Wong, J. K. *et al.* Recovery of replication-competent HIV despite prolonged suppression of plasma viremia. *Science (80-.).* **278**, 1291–1295 (1997).

4. Deeks, S. G. *et al.* A phase II randomized study of HIV-specific T-cell gene therapy in subjects with undetectable plasma viremia on combination antiretroviral therapy. *Mol. Ther.* **5**, 788–797 (2002).

5. Fernandez-Montero, J. V., Eugenia, E., Barreiro, P., Labarga, P. & Soriano, V. Antiretroviral drug-related toxicities-clinical spectrum, prevention, and management. *Expert Opinion on Drug Safety* vol. 12 697–707 (2013).

6. Iacob, S. A., Iacob, D. G. & Jugulete, G. Improving the Adherence to Antiretroviral Therapy, a Difficult but Essential Task for a Successful HIV Treatment—Clinical Points of View and Practical Considerations. *Front. Pharmacol.* **8**, 831 (2017).

7. Johnson Lyons, S. *et al.* Monitoring Selected National HIV Prevention and Care Objectives by Using HIV Surveillance Data—United States and 6 Dependent Areas, 2019. *HIV Surveill. Suppl. Rep.* **26**,.

8. Montessori, V., Press, N., Harris, M., Akagi, L. & Montaner, J. S. G. Adverse effects of antiretroviral therapy for HIV infection. *CMAJ* **170**, 229–38 (2004).

9. Reust, C. E. Common adverse effects of antiretroviral therapy for HIV disease. *Am. Fam. Physician* **83**, 1443–1451 (2011).

10. WHO | HIV drug resistance. *WHO* (2019).

11. Ndung'u, T., McCune, J. M. & Deeks, S. G. Why and where an HIV cure is needed and how it might be achieved. *Nature* vol. 576 397–405 (2019).

12. Liu, L. *et al.* Novel CD4-Based Bispecific Chimeric Antigen Receptor Designed for Enhanced Anti-HIV Potency and Absence of HIV Entry Receptor Activity. *J. Virol.* **89**, 6685–6694 (2015).

13. Katlama, C. *et al.* Barriers to a cure for HIV: New ways to target and eradicate HIV-1 reservoirs. *The Lancet* vol. 381 2109–2117 (2013).

14. Siliciano, J. D. & Siliciano, R. F. Recent developments in the search for a cure for HIV-1 infection: Targeting the latent reservoir for HIV-1. *Journal of Allergy and Clinical Immunology* vol. 134 12–19 (2014).

15. Lewin, S. R., Deeks, S. G. & Barré-Sinoussi, F. Towards a cure for HIV-are we making progress? *The Lancet* vol. 384 209–211 (2014).

16. Archin, N. M. & Margolis, D. M. Emerging strategies to deplete the HIV reservoir. *Current Opinion in Infectious Diseases* vol. 27 29–35 (2014).

17. Ananworanich, J. & Fauci, A. S. HIV cure research: a formidable challenge. *J. virus Erad.* **1**, 1–3 (2015).

18. Neelapu, S. S. *et al.* Axicabtagene Ciloleucel CAR T-Cell Therapy in Refractory Large B-Cell Lymphoma. *N. Engl. J. Med.* **377**, 2531–2544 (2017).

19. Maude, S. L. *et al.* Tisagenlecleucel in Children and Young Adults with B-Cell Lymphoblastic Leukemia. *N. Engl. J. Med.* **378**, 439–448 (2018).

20. Schuster, S. J. *et al.* Tisagenlecleucel in Adult Relapsed or Refractory Diffuse Large B-Cell Lymphoma. *N. Engl. J. Med.* **380**, 45–56 (2019).

21. Li, C., Mei, H. & Hu, Y. Applications and explorations of CRISPR/Cas9 in CAR T-cell therapy. *Brief. Funct. Genomics* **19**, 175–182 (2020).

22. Depil, S., Duchateau, P., Grupp, S. A., Mufti, G. & Poirot, L. 'Off-the-shelf' allogeneic CAR T cells: development and challenges. *Nat. Rev. Drug Discov.* **19**, 185–199 (2020).

23. Ghanem, M. H. *et al.* Bispecific chimeric antigen receptors targeting the CD4 binding site and high-mannose Glycans of gp120 optimized for anti–human immunodeficiency virus potency and breadth with minimal immunogenicity. *Cytotherapy* **20**, 407–419 (2018).

24. Folkvord, J. M., Armon, C. & Connick, E. Lymphoid Follicles Are Sites of Heightened Human Immunodeficiency Virus Type 1 (HIV-1) Replication and Reduced Antiretroviral Effector Mechanisms. *AIDS Res. Hum. Retroviruses* **21**, 363–370 (2005).

25. Hufert, F. T. *et al.* Germinal centre CD4+ T cells are an important site of HIV replication in vivo. *AIDS* **11**, 849–57 (1997).

26. Connick, E. *et al.* CTL Fail to Accumulate at Sites of HIV-1 Replication in Lymphoid Tissue. *J. Immunol.* **178**, 6975–6983 (2007).

27. Connick, E. *et al.* Compartmentalization of Simian Immunodeficiency Virus Replication within Secondary Lymphoid Tissues of Rhesus Macaques Is Linked to Disease Stage and Inversely Related to Localization of Virus-Specific CTL. *J. Immunol.* **193**, 5613–5625 (2014).

28. Tenner-Racz, K. *et al.* The unenlarged lymph nodes of HIV-1-infected, asymptomatic patients with high CD4 T cell counts are sites for virus replication and CD4 T cell proliferation. The impact of highly active antiretroviral therapy. *J. Exp. Med.* **187**, 949–959 (1998).

29. Biberfeld, P. *et al.* HTLV-III expression in infected lymph nodes and relevance to pathogenesis of lymphadenopathy. *Am. J. Pathol.* **125**, 436–442 (1986).

30. Brenchley, J. M. *et al.* Differential infection patterns of CD4+ T cells and lymphoid tissue viral burden distinguish progressive and nonprogressive lentiviral infections. *Blood* **120**, 4172–81 (2012).

31. Perreau, M. *et al.* Follicular helper T cells serve as the major CD4 T cell compartment for HIV-1 infection, replication, and production. *J. Exp. Med.* **210**, 143–56 (2013).

32. Fukazawa, Y. *et al.* B cell follicle sanctuary permits persistent productive simian immunodeficiency virus infection in elite controllers. *Nat. Med.* **21**, 132–9 (2015).

33. Pope, M. & Haase, A. T. Transmission, acute HIV-1 infection and the quest for strategies to prevent infection. *Nature Medicine* vol. 9 847–852 (2003).

34. Pantaleo, G. *et al.* HIV infection is active and progressive in lymphoid tissue during the clinically latent stage of disease. *Nature* **362**, 355–8 (1993).

35. Embretson, J. *et al.* Massive covert infection of helper T lymphocytes and macrophages by HIV during the incubation period of AIDS. *Nature* **362**, 359–362 (1993).

36. Schacker, T. *et al.* Rapid Accumulation of Human Immunodeficiency Virus (HIV) in Lymphatic Tissue Reservoirs during Acute and Early HIV Infection: Implications for Timing of Antiretroviral Therapy. *J. Infect. Dis.* **181**, 354–357 (2000).

37. Haase, A. T. *et al.* Quantitative image analysis of HIV-1 infection in lymphoid tissue. *Science* **274**, 985–9 (1996).

38. Fox, C. H. *et al.* Lymphoid germinal centers are reservoirs of human immunodeficiency virus type 1 RNA. *J. Infect. Dis.* **164**, 1051–1057 (1991).

39. Heath, S. L., Tew, J. G., Szakal, A. K. & Burton, G. F. Follicular dendritic cells and human immunodeficiency virus infectivity. *Nature* vol. 377 740–4 (1995).

40. Smith-Franklin, B. A. *et al.* Follicular Dendritic Cells and the Persistence of HIV Infectivity: The Role of Antibodies and Fcγ Receptors. *J. Immunol.* **168**, 2408–2414 (2002).

41. Joling, P. *et al.* Binding of human immunodeficiency virus type-1 to follicular dendritic cells in vitro is complement dependent. *J. Immunol.* **150**, (1993).

42. Tjernlund, A. *et al.* In situ detection of Gag-specific CD8+ cells in the GI tract of SIV infected Rhesus macaques. *Retrovirology* **7**, 12 (2010).

43. Sasikala-Appukuttan, A. K. *et al.* Location and Dynamics of the Immunodominant CD8 T Cell Response to SIVΔnef Immunization and SIVmac251 Vaginal Challenge. *PLoS One* **8**, e81623 (2013).

44. Li, S. *et al.* Low levels of siv-specific CD8+ T cells in germinal centers characterizes acute SIV infection. *PLoS Pathog.* **15**, (2019).

45. Li, Q. *et al.* Visualizing antigen-specific and infected cells in situ predicts outcomes in early viral infection. *Science* **323**, 1726–9 (2009).

46. Li, S. *et al.* Simian Immunodeficiency Virus-Producing Cells in Follicles Are Partially Suppressed by CD8+ Cells In Vivo. *J. Virol.* **90**, 11168–11180 (2016).

47. Förster, R. *et al.* A Putative Chemokine Receptor, BLR1, Directs B Cell Migration to Defined Lymphoid Organs and Specific Anatomic Compartments of the Spleen. *Cell* **87**, 1037–1047 (1996).

48. Schaerli, P. *et al.* CXC chemokine receptor 5 expression defines follicular homing T cells with B cell helper function. *J. Exp. Med.* **192**, 1553–62 (2000).

49. Haynes, N. M. *et al.* Role of CXCR5 and CCR7 in follicular Th cell positioning and appearance of a programmed cell death gene-1high germinal center-associated subpopulation. *J. Immunol.* **179**, 5099–108 (2007).

50. Quigley, M. F., Gonzalez, V. D., Granath, A., Andersson, J. & Sandberg, J. K. CXCR5+ CCR7- CD8 T cells are early effector memory cells that infiltrate tonsil B cell follicles. *Eur. J. Immunol.* **37**, 3352–3362 (2007).

51. Gunn, M. D. *et al.* A B-cell-homing chemokine made in lymphoid follicles activates Burkitt's lymphoma receptor-1. *Nature* **391**, 799–803 (1998).

52. Legler, D. F. *et al.* B cell-attracting chemokine 1, a human CXC chemokine expressed in lymphoid tissues, selectively attracts B lymphocytes via BLR1/CXCR5. *J. Exp. Med.* **187**, 655–660 (1998).

53. Havenar-Daughton, C. *et al.* CXCL13 is a plasma biomarker of germinal center activity. *Proc. Natl. Acad. Sci. U. S. A.* **113**, 2702–2707 (2016).

54. Chang, J. E. & Turley, S. J. Stromal infrastructure of the lymph node and coordination of immunity. *Trends in Immunology* vol. 36 30–39 (2015).

55. Katakai, T. *et al.* Organizer-Like Reticular Stromal Cell Layer Common to Adult Secondary Lymphoid Organs. *J. Immunol.* **181**, 6189–6200 (2008).

56. Katakai, T. Marginal reticular cells: a stromal subset directly descended from the lymphoid tissue organizer. *Front. Immunol.* **3**, 200 (2012).

57. Wang, X. *et al.* Follicular dendritic cells help establish follicle identity and promote B cell retention in germinal centers. *J. Exp. Med.* **208**, 2497–2510 (2011).

58. Kroenke, M. A. *et al.* Bcl6 and Maf Cooperate To Instruct Human Follicular Helper CD4 T Cell Differentiation. *J. Immunol.* **188**, 3734–3744 (2012).

59. Rasheed, A.-U., Rahn, H.-P., Sallusto, F., Lipp, M. & Müller, G. Follicular B helper T cell activity is confined to CXCR5hiICOShi CD4 T cells and is independent of CD57

expression. *Eur. J. Immunol.* **36**, 1892–1903 (2006).

60. Ayala, V. I. *et al.* CXCR5-Dependent Entry of CD8 T Cells into Rhesus Macaque B-Cell Follicles Achieved through T-Cell Engineering. *J. Virol.* **91**, (2017).

61. Haran, K. P. *et al.* Simian Immunodeficiency Virus (SIV)-Specific Chimeric Antigen Receptor-T Cells Engineered to Target B Cell Follicles and Suppress SIV Replication. *Front. Immunol.* **9**, 1–12 (2018).

62. Skinner, P. J. Targeting reservoirs of HIV replication in lymphoid follicles with cellular therapies to cure HIV. *Adv. Cell Gene Ther.* **2**, e27 (2019).

63. Skinner, P. J. Overcoming the Immune Privilege of B cell Follicles to Cure HIV-1 Infection. **1**, 1–3 (2014).

64. Wang, F. *et al.* RNAscope: A novel in situ RNA analysis platform for formalin-fixed, paraffin-embedded tissues. *J. Mol. Diagnostics* **14**, 22–29 (2012).

65. Deleage, C. *et al.* Defining HIV and SIV Reservoirs in Lymphoid Tissues. *Pathog. Immun.* **1**, 68 (2016).

66. Vasquez, J. J. *et al.* Elucidating the Burden of HIV in Tissues Using Multiplexed Immunofluorescence and In Situ Hybridization: Methods for the Single-Cell Phenotypic Characterization of Cells Harboring HIV In Situ. *J. Histochem. Cytochem.* **66**, 427–446 (2018).

67. Ayala, V. I. *et al.* Adoptive Transfer of Engineered Rhesus Simian Immunodeficiency Virus-Specific CD8 + T Cells Reduces the Number of Transmitted/Founder Viruses Established in Rhesus Macaques . *J. Virol.* **90**, 9942–9952 (2016).

68. Randolph, G. J. CCR7: Unifying Disparate Journeys to the Lymph Node. *J. Immunol.* **196**, 3–4 (2016).

69. Förster, R. *et al.* CCR7 coordinates the primary immune response by establishing functional microenvironments in secondary lymphoid organs. *Cell* **99**, 23–33 (1999).

70. Pampusch, M. S. *et al.* Rapid Transduction and Expansion of Transduced T Cells with Maintenance of Central Memory Populations. *Mol. Ther. - Methods Clin. Dev.* **16**, 1–10 (2020).

71. Bronnimann, M. P., Skinner, P. J. & Connick, E. The B-cell follicle in HIV infection: Barrier to a cure. *Front. Immunol.* **9**, 1–13 (2018).

72. Mylvaganam, G. H. *et al.* Dynamics of SIV-specific CXCR5+ CD8 T cells during chronic SIV infection. *Proc. Natl. Acad. Sci. U. S. A.* **114**, (2017).

73. Li, S. *et al.* Simian immunodeficiency virus-producing cells in follicles are partially suppressed by CD8+ cells in vivo. *J. Virol.* **90**, (2016).

74. He, R. *et al.* Follicular CXCR5-expressing CD8+ T cells curtail chronic viral infection. (2016) doi:10.1038/nature19317.

75. Younan, P. M. *et al.* Lentivirus-mediated gene transfer in hematopoietic stem cells is impaired in SHIV-infected, ART-treated nonhuman primates. *Mol. Ther.* **23**, 943–951 (2015).

76. Ollerton, M. T., Berger, E. A., Connick, E. & Burton, G. F. HIV-1-Specific Chimeric Antigen Receptor T Cells Fail To Recognize and Eliminate the Follicular Dendritic Cell HIV Reservoir In Vitro . *J. Virol.* **94**, (2020).

77. Bitton, N., Verrier, F., Debré, P. & Gorochov, G. Characterization of T cell-expressed chimeric receptors with antibody-type specificity for the CD4 binding site of HIV-1 gp120. *Eur. J. Immunol.* **28**, 4177–4187 (1998).

78. Romeo, C. & Seed, B. Cellular immunity to HIV activated by CD4 fused to T cell or Fc

receptor polypeptides. *Cell* **64**, 1037–1046 (1991).

79.   Sahu, G. K. *et al.* Anti-HIV designer T cells progressively eradicate a latently infected cell line by sequentially inducing HIV reactivation then killing the newly gp120-positive cells. *Virology* **446**, 268–275 (2013).

80.   Qi, J., Ding, C., Jiang, X. & Gao, Y. Advances in Developing CAR T-Cell Therapy for HIV Cure. *Front. Immunol.* **11**, 1–13 (2020).

81.   Brenchley, J. M. *et al.* CD4+ T cell depletion during all stages of HIV disease occurs predominantly in the gastrointestinal tract. *J. Exp. Med.* **200**, 749–759 (2004).

82.   Kalos, M. *et al.* T cells with chimeric antigen receptors have potent antitumor effects and can establish memory in patients with advanced leukemia. *Sci. Transl. Med.* **3**, 95ra73 (2011).

83.   Kalos, M. Biomarkers in T cell therapy clinical trials. *Journal of Translational Medicine* vol. 9 138 (2011).

84.   Porter, D., Levine, B., Kalos, M., Bagg, A. & June, C. H. Chimeric Antigen Receptor–Modified T Cells in Chronic Lymphoid Leukemia. *N. Engl. J. Med.* **365**, 725–733 (2011).

85.   Taraseviciute, A. *et al.* Chimeric antigen receptor T cell–mediated neurotoxicity in nonhuman primates. *Cancer Discov.* **8**, 750–763 (2018).

86.   Bolton, D. L. *et al.* Trafficking, persistence, and activation state of adoptively transferred allogeneic and autologous Simian Immunodeficiency Virus-specific CD8(+) T cell clones during acute and chronic infection of rhesus macaques. *J. Immunol.* **184**, 303–14 (2010).

87.   Minang, J. T. *et al.* Distribution, persistence, and efficacy of adoptively transferred central and effector memory-derived autologous simian immunodeficiency virus-specific CD8+ T cell clones in rhesus macaques during acute infection. *J. Immunol.* **184**, 315–326 (2010).

88.   Strongin, Z. *et al.* Virologic and Immunologic Features of Simian Immunodeficiency Virus Control Post-ART Interruption in Rhesus Macaques. *J. Virol.* **94**, (2020).

89.   Borducchi, E. N. *et al.* Ad26/MVA therapeutic vaccination with TLR7 stimulation in SIV-infected rhesus monkeys. *Nature* **540**, 284–287 (2016).

90.   Ayala, V. I. *et al.* Adoptive Transfer of Engineered Rhesus Simian Immunodeficiency Virus-Specific CD8 T Cells Reduces the Number of Transmitted/ Founder Viruses Established in Rhesus Macaques. (2016) doi:10.1128/JVI.01522-16.

91.   Anasetti, C. & Mulé, J. J. To ablate or not to ablate? HSCs in the T cell driver's seat. *Journal of Clinical Investigation* vol. 117 306–310 (2007).

92.   June, C. H. Adoptive T cell therapy for cancer in the clinic. *Journal of Clinical Investigation* vol. 117 1466–1476 (2007).

93.   Greenberg, P. D. Adoptive T cell therapy of tumors: Mechanisms operative in the recognition and elimination of tumor cells. *Adv. Immunol.* **49**, 281–355 (1991).

94.   Dudley, M. E. *et al.* Cancer regression and autoimmunity in patients after clonal repopulation with antitumor lymphocytes. *Science (80-.).* **298**, 850–854 (2002).

95.   Sengupta, S. & Siliciano, R. F. Targeting the Latent Reservoir for HIV-1. *Immunity* vol. 48 872–895 (2018).

96.   Mu, W., Carrillo, M. A. & Kitchen, S. G. Engineering CAR T Cells to Target the HIV Reservoir. *Front. Cell. Infect. Microbiol.* **10**, 410 (2020).

97.   Webb, G. M. *et al.* The human IL-15 superagonist ALT-803 directs SIV-specific CD8+ T cells into B-cell follicles. *Blood Adv.* **2**, 76–84 (2018).

98.   Pampusch, M. S. & Skinner, P. J. Transduction and expansion of primary T cells in nine days with maintenance of central memory phenotype. *J. Vis. Exp.* **2020**, 60400 (2020).

5

99. Nichole Cline, A., Bess, J. W., Piatak, M. J. & Lifson, J. D. Highly sensitive SIV plasma viral load assay: practical considerations, realistic performance expectations, and application to reverse engineering of vaccines for AIDS. *J. Med. Primatol.* **34**, 303–312 (2005).

100. Bertram, K. M. *et al.* Identification of HIV transmitting CD11c+ human epidermal dendritic cells. *Nat. Commun.* **10**, 1–15 (2019).

101. Abdelaal, H. M. *et al.* Comparison of Vibratome and Compresstome sectioning of fresh primate lymphoid and genital tissues for in situ MHC-tetramer and immunofluorescence staining. *Biol. Proced. Online* **17**, 2 (2015).

102. Skinner, P. J., Daniels, M. a., Schmidt, C. S., Jameson, S. C. & Haase, a. T. Cutting Edge: In Situ Tetramer Staining of Antigen-Specific T Cells in Tissues. *J. Immunol.* **165**, 613–617 (2000).

103. Li, S., Mwakalundwa, G. & Skinner, P. J. In situ MHC-tetramer staining and quantitative analysis to determine the location, abundance, and phenotype of antigen-specific CD8 T cells in tissues. *J. Vis. Exp.* **2017**, 1–8 (2017).

104. Abdelaal, H. M., Cartwright, E. K. & Skinner, P. J. Detection of Antigen-Specific T Cells Using In Situ MHC Tetramer Staining. *Int. J. Mol. Sci.* **20**, (2019).

Figure Legends

Fig 1. CAR/CXCR5-T cells home to lymphoid follicles and recognize SIV-infected cells in vivo. Location of cell trace violet (CTV)-labeled CAR/CXCR5-T cells was determined in a chronically SIV-infected ART-naïve rhesus macaque, animal R14025 at 2 days post-treatment (DPT). (a) Representative images from spleen, lymph node (LN), bone marrow, ileum, lung, liver, brain, and rectum. Infused cells were labeled with CTV (pseudo-colored red). Tissues were stained with anti-IgM or anti-CD20 (green) to label B cells and delineate B cell follicles (green). Arrowheads point to CTV-labeled cells. Scale bars=100 μm. (b) Representative image of spleen tissue section from animal R14025 showing duplex detection of CAR/CXCR5 construct (red) and SIV (pseudo-colored white) using RNAscope ISH combined with immunofluorescence using a custom-made probe for detection of CAR/CXCR5 construct and a probe specific for SIV. The white haze within the B cell follicle represents SIV virions trapped by the follicular dendritic cells (FDC) network. Scale bar=100 μm. The right panels of panel (b) are enlargements showing an interaction between two CAR/CXCR5-transduced T cells and an SIV-infected cell. The tissue was stained with DAPI (blue), and anti-CD20 (green) to label B cells and delineate B cell follicles. Scale bar=10 μm. Confocal images were collected using a 20× objective. The curves tool in Photoshop was used to increase the contrast of each image in a similar manner.

Fig 2. A timeline of the Rhesus macaque pilot studies. Animals were infected with SIV mac251 and ART suppressed. Cells were collected for transduction either post-infection (T1) or pre-infection (T2). ART was interrupted at the time of CAR/CXCR5 cell infusion. Blood and tissue samples were collected at regular intervals post-infusion.

7

Fig 3. Post-infusion viral loads. Viral loads over time in (a) untreated control animals, (b) pilot study T1 animals and (c) pilot study T2 animals. Viral loads were determined by measurement of gag mRNA relative to the housekeeping gene beta-actin in cell pellets using reverse transcription (RT) polymerase chain reaction (PCR). (d) Viral loads for the three animal groups one month post-infusion (27-30 DPI). The bar represents the median.

Fig 4. CAR/CXCR5-T cells continue to expand in vivo. CAR/CXCR5-T cells expanded at the edges of B cell follicles in vivo at 2 DPT and accumulated within B cell follicles at 6 DPT**.** (a) Representative image from LN tissue from Rh2850 stained 2 DPT showing CAR/CXCR5-T cell proliferation in the extrafollicular (EF) area near the follicular (F) zone. Tissues were stained with anti-CD3 (blue) to label T cells and anti-CD20 (green) to label B cells and delineate B cell follicles (F). CAR/CXCR5-infused cells were labeled with CTV (pseudo-colored red). Cells within F showed lower fluorescence intensity indicating division. Scale bar=50 μm. (b) Representative image of LN tissue section, from Rh2858 visualized using RNAScope ISH combined with IF, showing expansion of CAR/CXCR5-T cells at the edge of follicles at 2 DPT. The right panel is an enlargement from left panel showing a cluster of CAR/CXCR5-T cells (red) that appear to be expanding at the edge of the follicle. Tissues were stained with DAPI (blue) and anti-IgM (green) to label B cells and delineate B cell follicles (F), with the more brightly stained germinal center in the center of the F. (c) Representative image of LN tissue from Rh2850, showing CAR/CXCR5-T cell (red) proliferation in F and EF at 6 DPT detected by RNAScope ISH combined with IF. Tissues were stained with anti-IgM (Blue) and anti-Ki67 (green) to mark activation and proliferation. B cell follicles are delineated with white lines. Scale bars=100 μm.

8

Confocal images were collected using a 20× objective. (d) Percentage of Ki67+ CAR/CXCR5 T cells in the F (green) and EF (blue) areas for each of the T2 animals.

Fig 5. CAR/CXCR5-T cells localize to over 90% of the follicles and persist for up to 28 days. CAR/CXCR5-T cells successfully homed to over 90% of the B cell follicles at 6 DPT and persisted for up to 28 DPT in SIV-infected ART-suppressed/released animals. Representative images of LN tissue section from Rh2858, showing CAR/CXCR5-T cells (red) detected using RNAScope ISH combined with IF using a custom-made probe for detection of the CAR/CXCR5 construct. (a) Confocal image showing a whole LN tissue section. (b) Enlargement of the delineated area in (5a) showing that CAR/CXCR5-transduced T cells (red) successfully homed to a B cell follicle (green). The tissue was stained with DAPI (blue), and anti-CD20 (green) to label B cells and delineate B cell follicles. The confocal image is collected with a 20× objective. Scale bar=100 μm. (c) Levels of CAR/CXCR5-T cells over time after infusion in F (green) and EF areas (blue) of LN. The animal that lost control of the virus infection is marked with a red star. Samples not determined are marked ND. (d) Percentage of follicles that contained CAR/CXCR5-T cells over time post-infusion. (e) Frequency of CD4-MBL$^+$ cells in CD3$^+$ PBMCs as determined by flow cytometry and (f) copies of CAR in the total cell population in BAL as determined by quantitative real-time PCR at the indicated time points post-infusion.

Fig 6. Infusion of CAR/CXCR5-T cells into SIV-infected rhesus macaques results in lower viral loads post-ART interruption. At 28 DPT, treated animals showed a reduction in viral (v)RNA compared to untreated control animals. (a) A representative image from a LN tissue section showing the abundance of SIV vRNA$^+$ cells and free virions trapped by follicular dendritic cells network (pseudo-colored white) detected using RNAscope ISH combined with IF

9

in treated from Rh2850 (left panels) versus untreated control from R11002 (right panels). The

tissue was stained with DAPI (blue), and anti-CD20 (green) to label B cells and delineate B cell

follicles. The white haze within the B cell follicle represents SIV virions trapped by the follicular

dendritic cells (FDC) network. Confocal images were collected with a 20× objective. Scale bar

=100 μm. (b) Levels of viral RNA in F and EF areas. The animal that lost viral control of the

virus infection is marked with a red star. (c) The percentage of follicles with free virions bound

by FDC.

Supporting information

Fig S1. Immunotherapeutic cell infusion leads to transient increases in cytokine levels and cell accumulation in bronchoalveolar lavage fluid.

Serum samples were analyzed for post-infusion production of cytokines using a non-human primate (NHP)-specific (a) tumor necrosis factor (TNF) alpha, (b) interferon (IFN) gamma, (c) interleukin (IL)-6 and (d) IL-2 multiplex Luminex assay. Lung accumulation of CAR T cells was determined by analysis of bronchoalveolar lavage (BAL) samples. Cells were isolated from BAL and analyzed for (e) the percentage of CD4-MBL CAR$^+$ cells in the CD3$^+$ T population by flow cytometry or (f) the number of copies of CAR/cell in the total cell population by quantitative real-time PCR.

Fig S2. Representative flow plots from cells prepared for infusion. 1×10^6 cells were stained with the antibodies listed in the Flow Cytometry section of Materials and Methods. Gating strategy for determination of co-expression of CAR (MBL) and CXCR5. The CD8+ population was used to determine central memory phenotype (CD28$^+$CD95$^+$) and CCR7 expression. Plots presented are from cells infused into Rh2858.

Fig S3. Levels of tetramer$^+$ CD3 T cells present in peripheral blood mononuclear cells (PBMCs). PBMC, collected on d28 from animals in each of the three groups, were stained for Gag CM9 and analyzed by flow cytometry as described in Materials and Methods. The bar represents the median.

Fig S4. Numbers of follicular CAR/CXCR5-T cells identified in situ in lymph nodes correlate with numbers of CAR-specific PBMCs identified by flow cytometry.
Correlation between follicular CAR/CXCR5-T cells/mm^2 by RNAScope and CD4-MBL$^+$ PBMC by flow cytometry. Association was tested using Spearman's correlation. Scales are log (value+1) on the y-axis and log (value) on the x-axis; labels use the original units. The line represents the fitted regression.

a
CD20/IgM CTV labeled CAR/CXCR5 T cells

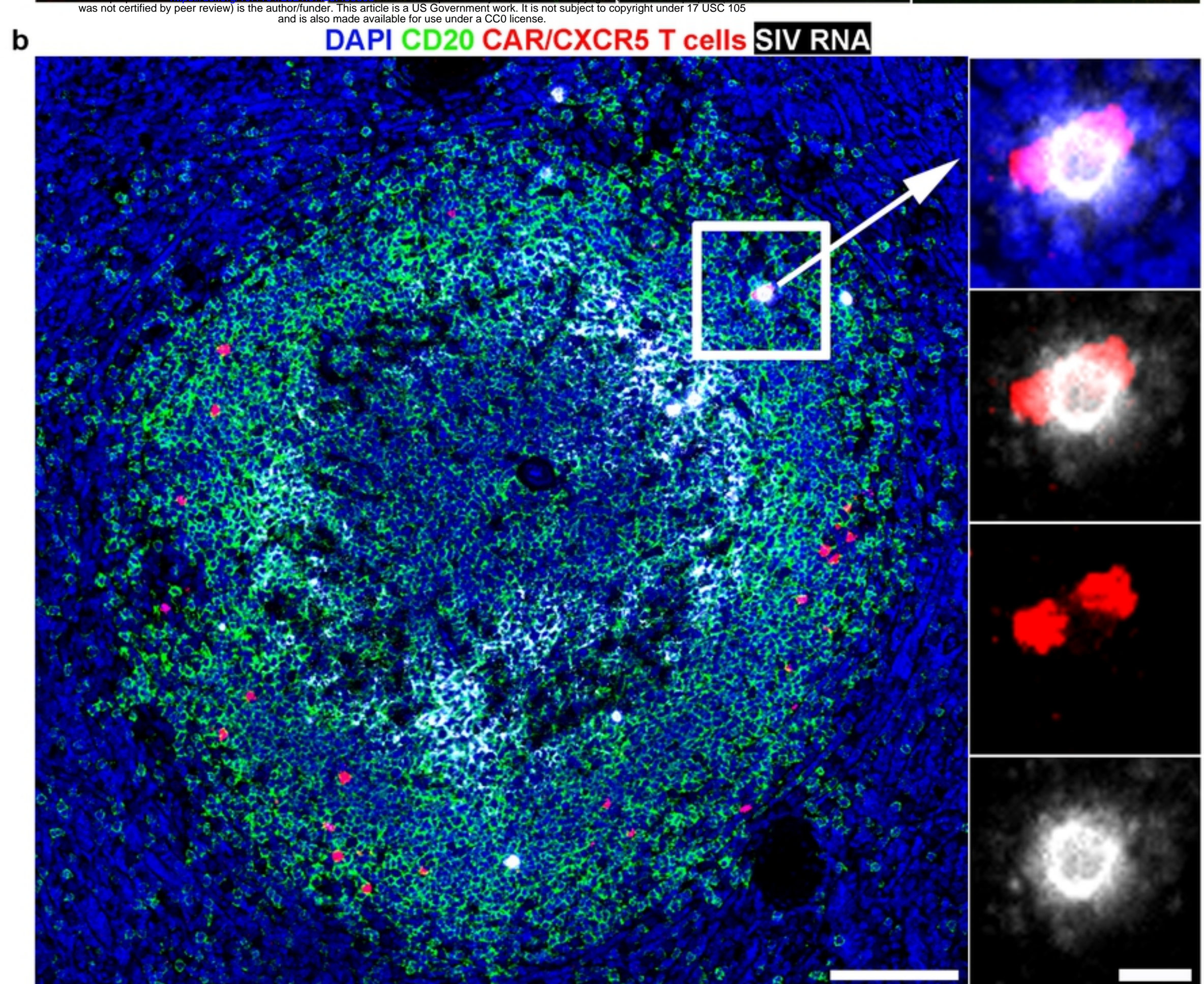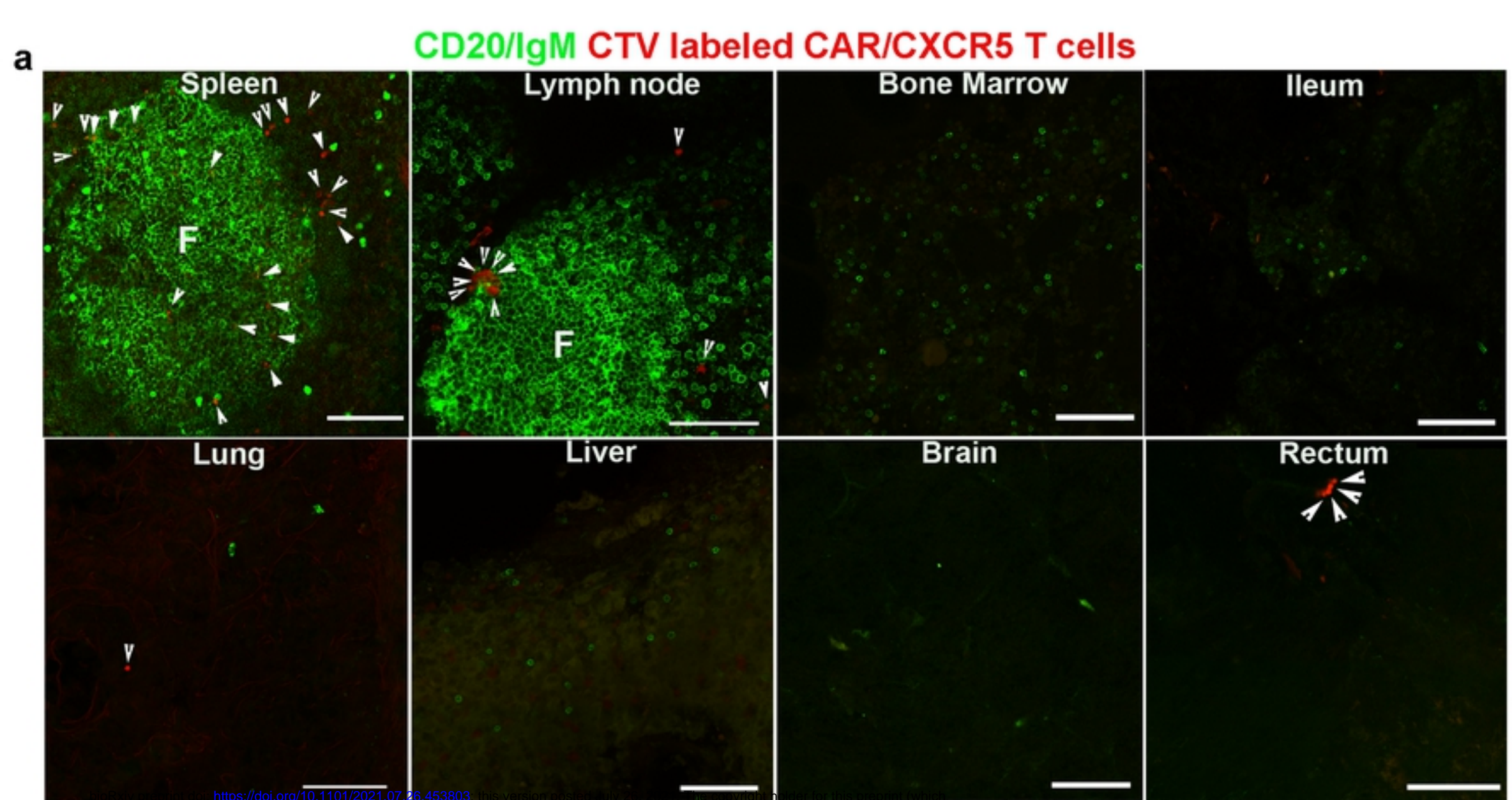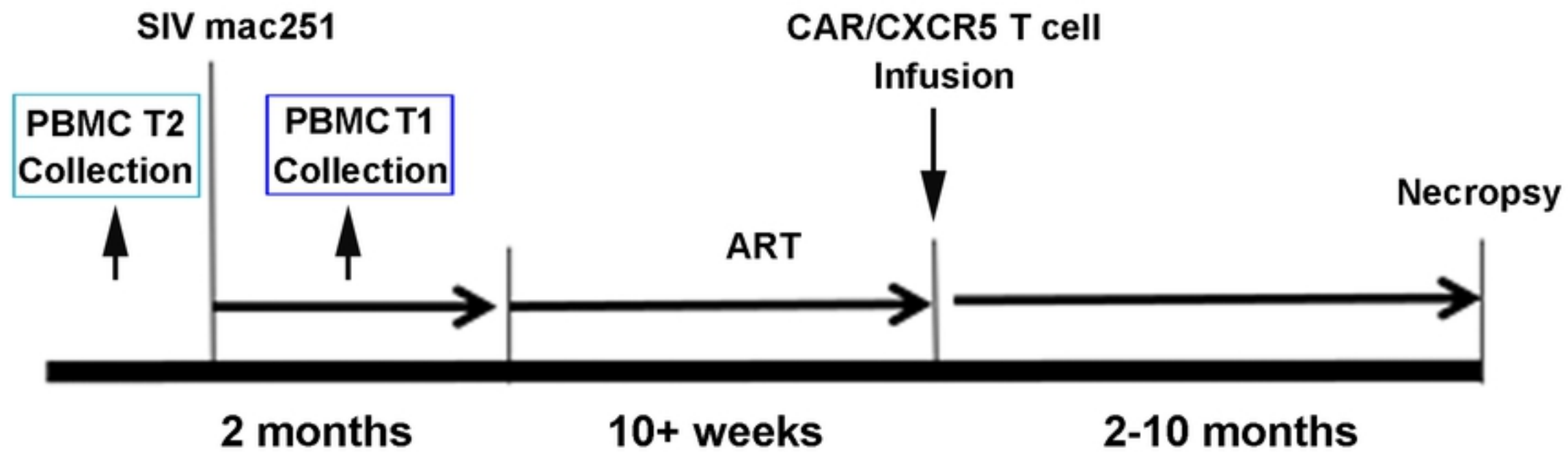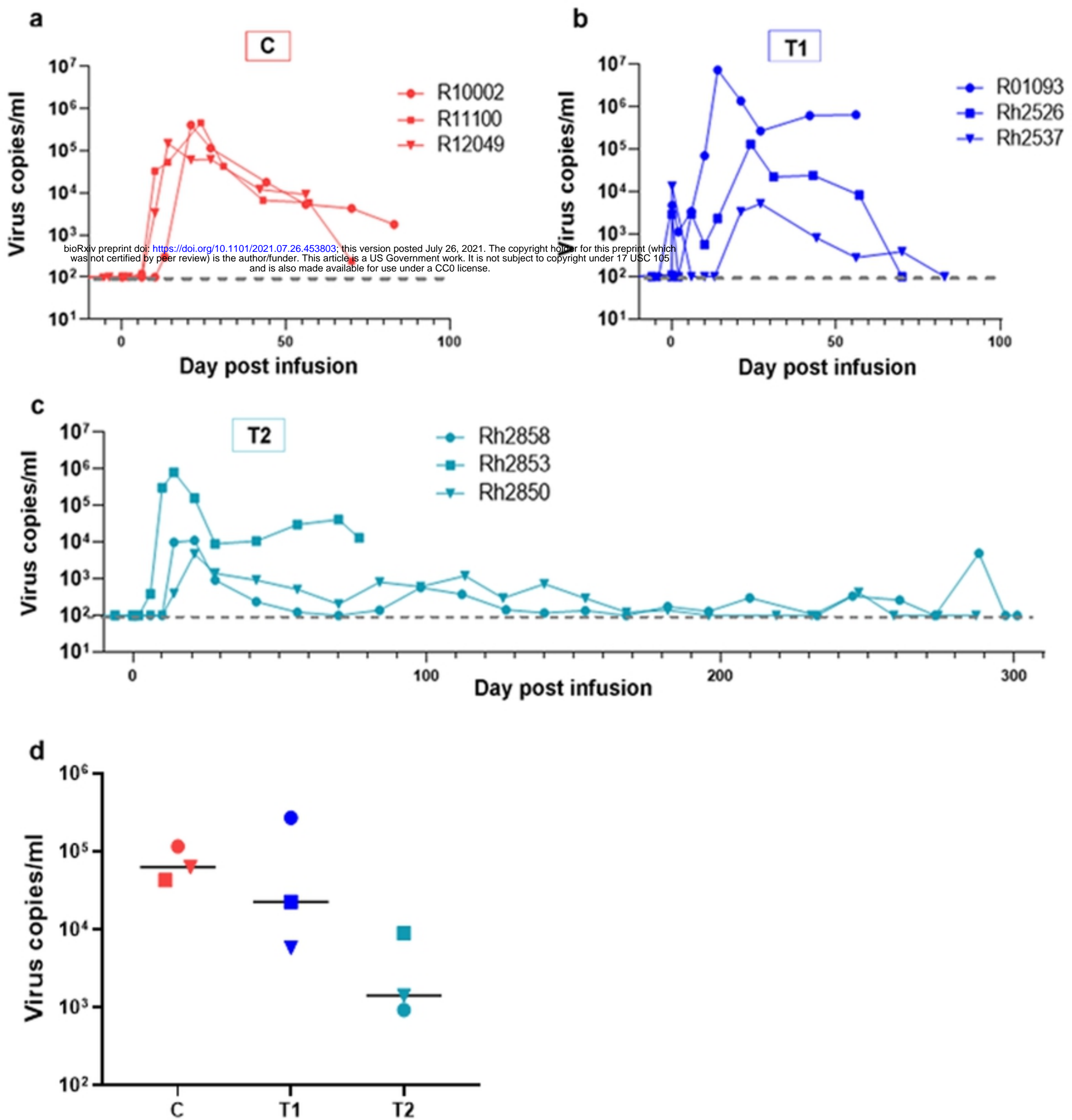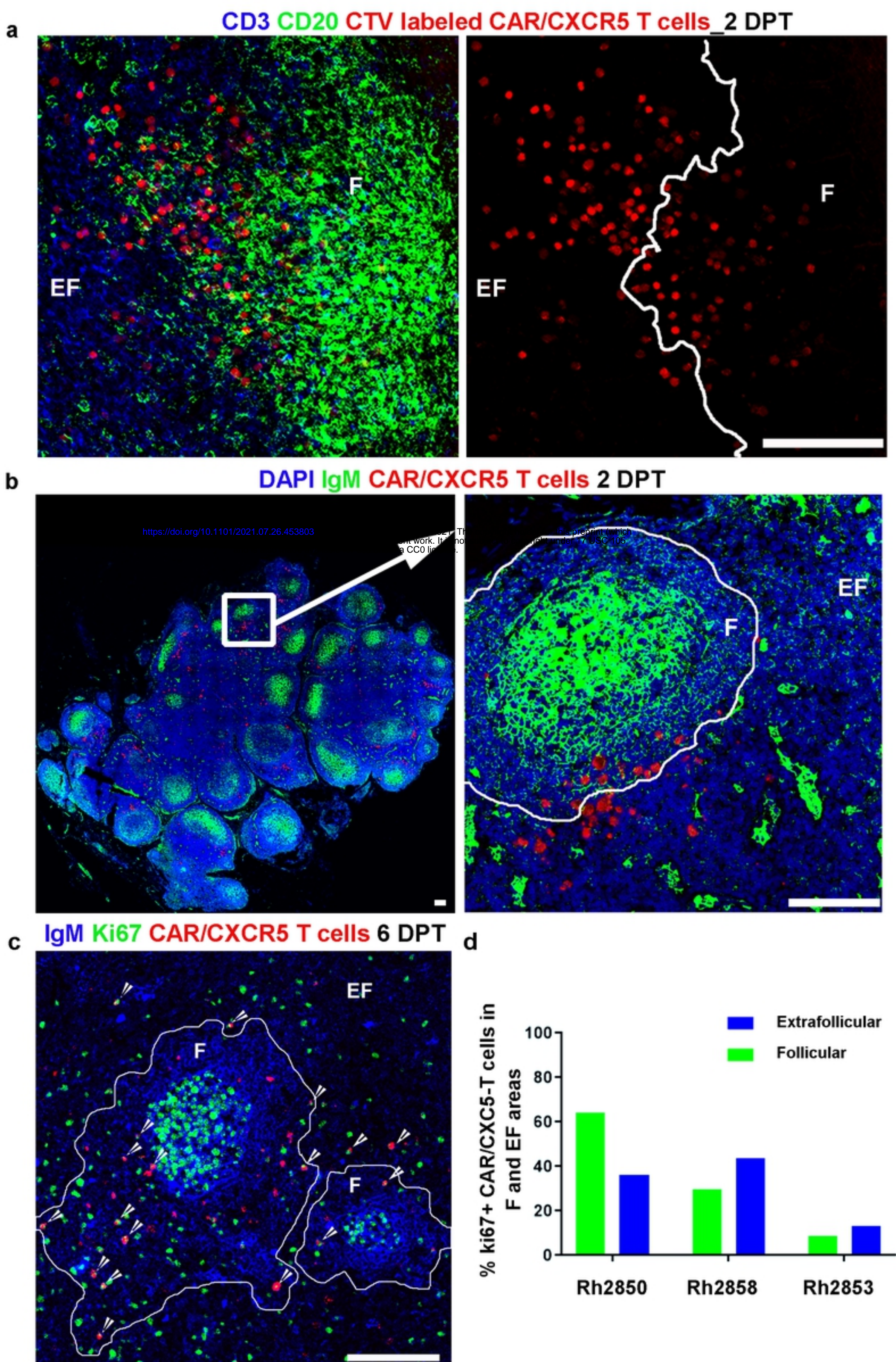Spleen | Lymph node | Bone Marrow | Ileum

Lung | Liver | Brain | Rectum

b
DAPI CD20 CAR/CXCR5 T cells SIV RNA

Figure 1

Figure 2

Figure 3

CD3 CD20 CTV labeled CAR/CXCR5 T cells_2 DPT

a

F

EF

EF

F

DAPI IgM CAR/CXCR5 T cells 2 DPT

b

EF

F

IgM Ki67 CAR/CXCR5 T cells 6 DPT

c

EF

F

F

d

% ki67+ CAR/CXC5-T cells in F and EF areas

Extrafollicular

Follicular

Rh2850   Rh2858   Rh2853

Figure 4

DAPI CD20 CAR/CXCR5 T cells 6 DPT

Figure 5

a

Treated `DAPI` `CD20` `SIV`   Untreated control `DAPI` `CD20` `SIV`

Treated `SIV`   Untreated control `SIV`

b

vRNA⁺ Cells/mm²

- ■ Extrafollicular
- ■ Follicular
- ✶ Lost control

Rh2850 Rh2858 Rh2853   R11000 R10002 R12049

Treated   Untreated control

C

% F with FDC⁺ free virions

✶ Lost control

0/16 1/30 30/36   22/24 11/21 21/31

Rh2850 Rh2858 Rh2853   R11000 R10002 R12049

Treated   Untreated control

Figure 6